

Nonlinear enhanced mass sensor based on optomechanical system

Xin-Xin Man(满鑫鑫), Jing Sun(孙静), Wen-Zhao Zhang(张闻钊), Lijuan Luo(罗丽娟), and Guangri Jin(金光日)

Citation: Chin. Phys. B, 2024, 33 (**12**): 120303. DOI: 10.1088/1674-1056/ad84cf
Journal homepage: http://cpb.iphy.ac.cn; http://iopscience.iop.org/cpb

What follows is a list of articles you may be interested in

Nonreciprocal mechanical entanglement in a spinning optomechanical system

Shan-Shan Chen(陈珊珊), Jing-Jing Zhang(张京京), Jia-Neng Li(李嘉能), Na-Na Zhang(张娜娜), Yong-Rui Guo(郭永瑞), and Huan Yang(杨桓)

Chin. Phys. B, 2024, 33 (**11**): 110305. DOI: 10.1088/1674-1056/ad72e1

Nonlinearly induced entanglement in dissipatively coupled optomechanical system

Wen-Quan Yang(杨文全), Xuan Leng(冷轩), Jiong Cheng(程泂), and Wen-Zhao Zhang(张闻钊)

Chin. Phys. B, 2024, 33 (**6**): 060313. DOI: 10.1088/1674-1056/ad3dd6

Direct measurement of two-qubit phononic entangled states via optomechanical interactions

A-Peng Liu(刘阿鹏), Liu-Yong Cheng(程留永), Qi Guo(郭奇), Shi-Lei Su(苏石磊), Hong-Fu Wang(王洪福), and Shou Zhang(张寿)

Chin. Phys. B, 2022, 31 (**8**): 080307. DOI: 10.1088/1674-1056/ac5d2f

Photon blockade in a cavity-atom optomechanical system

Zhong Ding(丁忠) and Yong Zhang(张勇)

Chin. Phys. B, 2022, 31 (**7**): 070304. DOI: 10.1088/1674-1056/ac4cbc

Topological phase transition in cavity optomechanical system with periodical modulation

Zhi-Xu Zhang(张志旭), Lu Qi(祁鲁), Wen-Xue Cui(崔文学), Shou Zhang(张寿), and Hong-Fu Wang(王洪福)

Chin. Phys. B, 2022, 31 (**7**): 070301. DOI: 10.1088/1674-1056/ac4a6a

---

SPECIAL TOPIC — Quantum computing and quantum sensing

Nonlinear enhanced mass sensor based on optomechanical system

Xin-Xin Man(满鑫鑫)[1,2], Jing Sun(孙静)[3], Wen-Zhao Zhang(张闻钊)[3], Lijuan Luo(罗丽娟)[2,†], and Guangri Jin(金光日)[1,‡]

[1] *Key Laboratory of Optical Field Manipulation of Zhejiang Province and Physics Department of Zhejiang Sci-Tech University, Hangzhou* 310018, *China*
[2] *Department of Materials and Chemical Engineering, Ningbo University of Technology, Ningbo* 315211, *China*
[3] *School of Physical Science and Technology, Ningbo University, Ningbo* 315211, *China*

(Received 14 August 2024; revised manuscript received 3 October 2024; accepted manuscript online 9 October 2024)

A high-precision and tunable mass detection scheme based on a double-oscillator optomechanical system is proposed. By designating one of the oscillators as the detection port, tiny mass signals can be probed through the frequency shift of the output spectrum, utilizing the system's optomechanically induced transparency (OMIT) effect. By solving the output of the optical mode, we demonstrate that the system exhibits two OMIT windows due to the double-oscillator coupling, with one window being strongly dependent on the mass to be detected. Characterizing the spectrum around this window enables high magnification and precise detection of the input signal under nonlinear parameter conditions. Additionally, our scheme shows resilience to environmental temperature variations and drive strength perturbations.

Keywords: optomechanically induced transparency, optomechanical system, mass sensor

PACS: 03.67.Bg, 42.50.–p, 42.50.Wk **DOI:** 10.1088/1674-1056/ad84cf

1. Introduction

Quantum mechanics, when combined with advanced measurement technologies, has led to remarkable achievements such as gravitational wave detection,[1–3] dark matter searches,[4–6] and low-reflective object detection.[7–9] The integration of quantum technology has enabled detection capabilities that exceed the classical limits, reaching and even surpassing the standard quantum limit (SQL).[10–12] This breakthrough in detection technology opens up possibilities for tasks that classical technology cannot perform, such as microwave sensing at the subphoton level,[13] single spin detection,[14,15] and resolving vacuum fluctuations.[16] Among these advancements, the detection of tiny masses holds significant importance for various applications, including biospecimen detection[17] and addressing quantum–classical boundary problems.[18,19]

A high-precision quantum detection device based on optomechanics, which converts minute mass perturbations into optical signals, has garnered significant attention for its potential applications.[3,16,19–21] The optomechanical system naturally links the mechanical mode of a massive object with the optical mode, demonstrating excellent detection properties. The utilization of this system as a platform enables the detection of mechanical signals with optical precision.[22–24] When combined with homodyne detection technology, we can achieve high detection accuracy across various applications, including quantum illumination,[9,25] mechanical motion measurement,[26] and weak-field detection.[3,11] In mass sensing, optomechanical systems have demonstrated significant theoretical and experimental advantages,[17,27–29] including mass sensors based on four-wave mixing[17,27] and mass detection via mechanical oscillation frequency shifts.[28,29] However, the SQL constrains the potential for improving the detection accuracy in these protocols. Breakthroughs in surpassing the SQL of detection noise can be achieved by utilizing a coherent noise cancellation scheme.[11,30,31] The SQL is essentially a manifestation of the Heisenberg limit of the system.[19] To achieve precise measurements, the probe system must be dominated by quantum effects. This requires cooling the probe system to a temperature where environmental classical noise, such as thermal noise, can be ignored. Typically, this cooling occurs within the range of milli-Kelvin to Kelvin.[32,33] However, this low-temperature requirement significantly limits the implementation of detection schemes, particularly for biological samples like chromosomes and cellular assays,[34–36] where room temperature detection is essential. To address the need for room-temperature detection, various schemes have been proposed that perform well at room temperature or even temperature-robust, such as nonlinear optical mass sensors[17] and mass detection based on frequency shifts.[37] The core of these schemes is to exploit the difference in the system's response to signal and noise. This opens up the possibility of using differential effects, such as nonlinearities, as detection techniques to distinguish mass signals from noise. Optomechanically induced transparency (OMIT) is a typical nonlinear ef-

†Corresponding author. E-mail: lijuanluo1224@hotmail.com
‡Corresponding author. E-mail: grjin@zstu.edu.cn

© 2024 Chinese Physical Society and IOP Publishing Ltd

fect in optomechanical systems[38] and exhibits a range of remarkable quantum properties.[39–42] OMIT has been realized in various physical setups, including whispering gallery mode cavities,[43] membrane-in-the-middle systems,[44] and nano-electromechanical systems.[45] The potential advantages of OMIT for detection have been investigated, with several protocols developed for detecting the orbital angular momentum of light fields[46] as well as mass.[47,48] However, current OMIT-based mass sensing schemes depend on the linear relationship between mass-induced frequency shifts and the OMIT spectrum, resulting in detection accuracy that is solely determined by the system's mass responsivity, limiting effective signal amplification.

In this work, we design a double-mechanical mode optomechanical detection system by combining OMIT with mass detection. A tiny mass object is attached to one of the mechanical oscillators, causing a change in its intrinsic frequency. This frequency shift, induced by the attached mass, is reflected in the spectral window position of OMIT and can be detected through optical measurement. Additionally, through eigenfrequency resolution analysis, we identify the existence of a quasi-mode (defined as shift frequency mode) in the system, which is highly sensitive to mass changes (or frequency variations). The OMIT spectrum of the frequency-shifted mode directly reflects the mass of the attached object, allowing for temperature-robust detection of small masses within a specific range, as well as nonlinear amplification of signals in our scheme. The paper is organized as follows. In Section 2, we describe and solve the model we study and analyze the underlying mechanism of mass detection. In Section 3, we examine the OMIT effect of the output field and the mechanism of mode splitting. In Section 4, we present the scheme for tiny mass detection and discuss its detection capabilities. Finally, the summary and discussion are provided in Sections 5 and 6.

2. Model and Hamiltonian

The schematic diagram of our system is shown in Fig. 1. Both mirrors of the cavity are movable. One of the mirrors is used as the detection port to detect the mass of attached particles. The system's Hamiltonian takes the form

$$\frac{H}{\hbar}=\omega_a a^\dagger a+\sum_{j=1,2}\frac{\omega_{\mathrm{m}j}}{2}(p_j^2+q_j^2)-g_j a^\dagger a q_j+V q_1 q_2, \quad (1)$$

where a and $a^\dagger$ denote the annihilation and creation operators of the cavity, while q_j and p_j are the position and momentum operators of the j-th mechanical oscillator. g_j denotes the strength of the single-photon optomechaical coupling rate with the j-th mechanical resonator. V denotes the coupling strength between the two mechanical oscillators and can be realized via a substrate-mediated interaction in a high-stress silicon nitride membrane.[11,49] The system is simultaneously driven by a strong coupling field $\varepsilon_{\mathrm{c}}=\sqrt{2\kappa P_{\mathrm{c}}/\omega_{\mathrm{c}}}$ with frequency ω_{c} and weak probe field $\varepsilon_{\mathrm{p}}=\sqrt{2\kappa P_{\mathrm{p}}/\omega_{\mathrm{p}}}$ with frequency ω_{p}, where P_{c} and P_{p} denote the powers of the pump field and probe field, respectively. κ denotes the optical dissipation rate. The Hamiltonian of the driving can be written as

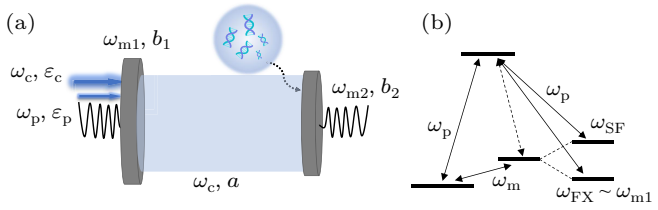


Fig. 1. Sketch of the studied system. (a) A strong coupling field at frequency ω_{c} and a weak probe field at frequency ω_{p} are injected into the cavity through the left mirror. Both mirrors of the cavity are movable. One of the mirrors is used as the detection port to detect the mass of attached particles. After the interaction between the cavity field and the mechanical oscillators, the output field will contain multiple frequencies. (b) Schematic diagram of the equivalent energy levels of an optomechanical system. A typical electomagnetically induced transparency (EIT) energy level structure is illustrated. Due to the coupling, the mechanical mode of the system splits into two quasi-modes, one of which is close to the original frequency (ω_{FX}) and the other is far away from it (ω_{SF}).

$$H_{\mathrm{d}}=\sum_{j=\mathrm{c,p}}\mathrm{i}\hbar\varepsilon_j(a^\dagger \mathrm{e}^{-\mathrm{i}\omega_j t}-a\mathrm{e}^{\mathrm{i}\omega_j t}). \quad (2)$$

In our model, we intend to measure the tiny mass as an example (such as chromosome-1 molecule[11,49]) where the external accretion mass will introduce an additional frequency response to the 2nd mechanical resonator. The purpose of introducing two oscillators is to use one of them as a reference and the other as a probe, and the effect caused by the relative frequency difference between them can be used as a detection basis. This approach can effectively avoid frequency perturbations caused by non-mechanical modes. The corresponding mass responsivity is defined as $\mathcal{R}=\partial\omega/\partial m$, with the typical value $\mathcal{R}=11\ \mathrm{Hz}\cdot\mathrm{yg}^{-1}$.[29,50] To implement our probe protocol, we deposit a few tiny mass particles onto the surface of the 2nd mechanical resonator. The signal introduced by the mass attachment can be described as $\Delta\omega=Nm\mathcal{R}$, where m and N are the mass and number of attached particles, respectively. Thus the eigenfrequency of the 2nd mechanical resonator should be modified as $\omega_{\mathrm{m2}}=\omega_{\mathrm{m0}}-\Delta\omega$, where ω_{m0} denotes the original frequency of the 2nd mechanical resonator without attached particles. To analyze the signal detection specifically, we need to solve the dynamics of the system. In the frame rotating at pump laser frequency ω_{c}, the quantum Langevin equations can be obtained as

$$\dot{a}=-(\mathrm{i}\Delta+\frac{\kappa}{2})a+\sum_{j=1,2}\mathrm{i}ag_j q_j+\varepsilon_{\mathrm{d}}+\sqrt{\kappa}a_{\mathrm{in}}, \quad (3a)$$

$$\dot{q}_j=\omega_{\mathrm{m}j}p_j, \quad (3b)$$

$$\dot{p}_j=-\omega_{\mathrm{m}j}q_j-\gamma_j p_j+g_j a^\dagger a-V q_{3-j}+\sqrt{\gamma_j}p_{\mathrm{in},j}, \quad (3c)$$

where $\varepsilon_{\rm d} = \varepsilon_{\rm c} + \varepsilon_{\rm p}\,{\rm e}^{-{\rm i}\delta t}$ is the total driving. $\Delta = \omega_a - \omega_{\rm c}$ is the cavity detuning, $\delta = \omega_{\rm p} - \omega_{\rm c}$ is the detuning between the probe field and the driving field. κ is the cavity decay rate and $a_{\rm in}$ is the vacuum radiation input noise operator of the cavity mode. γ_j is the mechanical decay rate and $p_{{\rm in},j}$ describes the input thermal noise. Under Born–Markov approximation we have $\langle p^{\dagger}_{{\rm in},j} p_{{\rm in},k}\rangle = n_{{\rm th},j}\delta(j,k)$, where $n_{{\rm th},j} = [\exp(\hbar\omega_{{\rm m}j}/k_{\rm B}T) - 1]^{-1}$ describes the equivalent thermal occupation.

Under strong driving and weak coupling conditions, the optical and mechanical operators can be split into the mean value and quantum fluctuation components: $a \to \delta a + \langle a\rangle$, $b_j \to \delta b_j + \langle b_j\rangle$, where $b_j = ({\rm i}p_j + q_j)/\sqrt{2}$ denotes the annihilation operator of the j-th mechanical oscillator. In the presence of a strong driving field, the photon and phonon numbers of the system are large enough, i.e., $\{\langle a\rangle, \langle b_j\rangle\} \gg \{\delta a, \delta b_j\}$. In this case, the transmission characteristics of the system is dominated by the mean value components, and the quantum fluctuation can be ignored. Thus, Eq. (3) is rewritten as

$$\langle \dot{a}\rangle = -\left[{\rm i}(\Delta - \sum_{j=1,2} g_j\langle q_j\rangle) + \frac{\kappa}{2}\right]\langle a\rangle + \varepsilon_{\rm d}, \tag{4a}$$

$$\langle \dot{q_j}\rangle = \omega_{{\rm m}j}\langle p_j\rangle, \tag{4b}$$

$$\langle \dot{p_j}\rangle = -\omega_{{\rm m}j}\langle q_j\rangle - \gamma_j\langle p_j\rangle + g_j\langle a^{\dagger}\rangle\langle a\rangle - V\langle q_{3-j}\rangle. \tag{4c}$$

In our model, the probe field is very weak and can be treated as a small quantity in the Hamiltonian. We thus can write each operator in the form of perturbation solution

$$\langle h\rangle = \langle h\rangle_0 + \langle h\rangle_+\varepsilon_{\rm p}\,{\rm e}^{-{\rm i}\delta t} + \langle h\rangle_-\varepsilon^*_{\rm p}\,{\rm e}^{{\rm i}\delta t} + {\rm O}[\varepsilon^2_{\rm p}]. \tag{5}$$

Ignoring the high order small quantity ${\rm O}[\varepsilon^2_{\rm p}]$, the steady-state solutions with $t \to \infty$ are obtained as

$$\langle a\rangle_0 = \frac{\varepsilon_{\rm c}}{{\rm i}\Delta' + \kappa/2}, \tag{6a}$$

$$\langle q_1\rangle_0 = \frac{|a_0|^2(g_1\omega_{\rm m2} - g_2 V)}{\omega_{\rm m1}\omega_{\rm m2} - V^2}, \tag{6b}$$

$$\langle q_2\rangle_0 = \frac{|a_0|^2(g_2\omega_{\rm m1} - g_1 V)}{\omega_{\rm m1}\omega_{\rm m2} - V^2}, \tag{6c}$$

$$\langle a\rangle_+ = \frac{{\rm i}\varepsilon_{\rm p}(\Gamma_1\Gamma_2 - V^2\omega_{\rm m1}\omega_{\rm m2})}{\Gamma_{\rm c}(\Gamma_1\Gamma_2 - V^2\omega_{\rm m1}\omega_{\rm m2}) - \Theta}, \tag{6d}$$

where

$$\Delta' = \Delta - \sum_{j=1,2} g_j\langle q_j\rangle_0,$$

$$\Theta = \sum_{j=1,2}\Gamma_{3-j}|G_j|^2\omega_{{\rm m}j} + G^*_j G_{3-j} V\omega_{\rm m1}\omega_{\rm m2},$$

in which $\Gamma_j = {\rm i}\gamma_j\delta + \delta^2 - \omega_{{\rm m}j}$, and $\Gamma_{\rm c} = {\rm i}\kappa/2 + \delta - \Delta$. $G_j = g_j\langle a\rangle_0$ denotes the Linearized coupling rate. The output field can be derived by using the input–output relation, where

$$\varepsilon_{\rm out} + \varepsilon_{\rm p}\,{\rm e}^{-{\rm i}\delta t} + \varepsilon_{\rm c} = \kappa\langle a\rangle. \tag{7}$$

It is obvious that the output spectrum is a function of $\omega_{\rm m2}$. Thus, the signal of the output field contains the information of the attached molecules. By measuring the transmission characteristics of the output field, we can obtain the mass or the number of the chromosome-1 molecules to be measured. According to the perturbative expansion form used previously, the output field can be extended in the form

$$\varepsilon_{\rm out} = \varepsilon_{\rm out0} + \varepsilon_{\rm out+}\varepsilon_{\rm p}\,{\rm e}^{-{\rm i}\delta t} + \varepsilon_{\rm out-}\varepsilon^*_{\rm p}\,{\rm e}^{{\rm i}\delta t}, \tag{8}$$

where $\varepsilon_{\rm out0}$, $\varepsilon_{\rm out+}$ and $\varepsilon_{\rm out-}$ correspond to the responses at the original frequencies $\omega_{\rm c}$, $\omega_{\rm p}$ and $2\omega_{\rm c} - \omega_{\rm p}$, respectively. Combing Eqs. (5), (7), and (8), we obtain

$$\varepsilon_{\rm out0} = \kappa\langle a\rangle_0 - \varepsilon_{\rm c},\ \ \varepsilon_{\rm out+} = \kappa\langle a\rangle_+ - 1,\ \ \varepsilon_{\rm out-} = \kappa\langle a\rangle_-. \tag{9}$$

The probe field can exhibit EIT-like behavior in the present strong coupling field in the optomechanical system.[51] We focus on the output field $\varepsilon_{\rm out+}$ with frequency $\omega_{\rm p}$. To investigate the transmission characteristics of $\varepsilon_{\rm out+}$, we define $\chi = \kappa\langle a\rangle_+$ to describe the response of the cavity optomechanical system to the probe field. According to the absorption and dispersion theory, the real part and imagery part of χ respectively represent the behaviors of absorption and dispersion.[52]

3. OMIT in output field

In this section, we investigate the relationship between the OMIT behavior of the output field and the small absorbed mass. Figure 2 illustrates the OMIT spectrum with different system parameters. Figure 2(a) shows the real and imagery parts of χ with different coupling strength V. The OMIT window is raised due to the optomechanical sideband effect.[43,53] This window is shifted to the high frequency range by enlarging the mechanical coupling strength, which can be understood by diagonalizing the coupled mechanical oscillator. In Fig. 2(b), we investigate the effect of the optomechanical coupling strength on the OMIT window. When $G_1 \neq G_2$, two OMIT windows are raised in the output field, i.e., positions where both the real and imaginary parts are 0. The value of G_2 has an effect on the frequency of OMIT windows. As G_2 increases, the peaks in the real part and the valleys in the imaginary part move, where those greater than $\omega_{\rm m1}$ move towards the high frequency part, and conversely those less than $\omega_{\rm m1}$ move towards the low frequency part, and the distance between these two peaks or valleys increases with the increase of G_2. When $G_1 = G_2$, the OMIT window in the low frequency disappears due to the decoupling of effective odd mode with low frequency under this condition. Thus, in our model the number of OMIT windows can be adjusted by the difference between G_1 and G_2, and the frequency of OMIT windows can be controlled by adjusting the value of V. As shown in Fig. 2(c), when the two oscillators are not identical, which

means there is a frequency difference between them, an extra OMIT window appears. As the frequency ω_{m2} decreases, both OMIT windows move away from the central frequency ω_{m1}, and the peaks and valleys of both the real and imaginary parts (absorption and dispersion) behave similarly. It is worth noting that the signal to be measured (small mass object) is also reflected in the output spectrum by the frequency change of ω_{m2}. Therefore, figure 2(a) can also intuitively show the characteristics of the signal detection spectrum. The position of OMIT window, peak value of real part or valley value of imaginary part can be used to calibrate the size of the signal. For OMIT, its position is robust to the linearized coupling strength. If the OMIT window is selected as the probe, the disturbance caused by the instability of driving strength can be resisted. The characteristics of the absorption peak and the dispersion valley are similar in the spectrum, and the absorption peak is more recognizable. If it is used as a probe, although it loses its robustness to the linearized coupling strength, its position is adjustable (Figs. 2(a) and 2(b) can be adjusted by altering the driving laser or the coupling between the mechanical oscillators). For example, we can control the position of the peak so that it appears in the highly sensitive area of detection (the detailed discussion will be given in Section 4). This high tunability of the OMIT window due to the dual-oscillator system and the dual-window property is beyond the capability of the conventional OMIT system. Especially for the double windows due to mode splitting, the change of their relative positions can reflect the magnitude of the mass adsorbed by the probe port oscillator.

As we mentioned in Section 2, the eigenfrequency of the 2nd mechanical resonator is modified by $\omega_{m2} \to \omega_{m0} - \delta\omega$ with absorbed mass. We have shown the OMIT windows of the output field with different ω_{m2} in Fig. 2(c). The lower window has a larger frequency shift than the higher window with the same ω_{m2} reduction. To understand the unbalanced frequency shift effect, we recall the equivalent energy level structure diagram shown in Fig. 1(b). Two obvious OMIT windows are raised in our model, which are respectively distributed on the left and right sides of ω_m. The OMIT window is split into two due to the coupling effect between the two oscillators. The corresponding polarized effective frequency can be obtained by diagonalization of the coupling oscillator

$$\omega_{\pm} = \frac{\omega_{m1} + \omega_{m2} \pm \sqrt{4V^2 + (\omega_{m1} - \omega_{m2})^2}}{2}. \tag{10}$$

According to the express of $\omega_{\pm}$, one can obtain that under condition $V \ll \omega_{m1,2}$, when $\omega_{m2} > \omega_{m1}$, $\omega_{FX,SF} = \omega \mp \approx \omega_{m1,2}$, when $\omega_{m2} < \omega_{m1}$, $\omega_{FX,SF} = \omega \pm \approx \omega_{m1,2}$. Thus, the window caused by ω_{SF} can directly reflect the frequency change of the detector oscillator ($\omega_{SF} \approx \omega_{m2}$). We mark it as shifted frequency ω_{SF}. And the window caused by $\omega_{FX} \approx \omega_{m1}$ does not respond well to the frequency change of the detection port. We mark it as fixed frequency ω_{FX}.

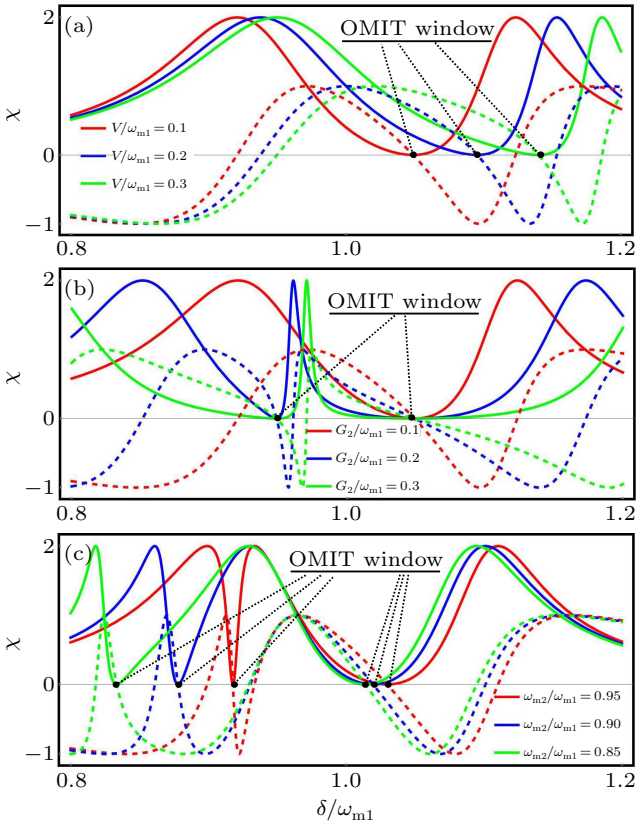


Fig. 2. OMIT behavior of the output field, the real part denotes the absorption of the optomechanical system to the prob field, the imagery part the dispersion of the optomechanical system to the prob field. (a) OMIT spectrum as a function of mechanical coupling strength V. (b) OMIT spectrum as a function of linearized coupling strength G_2. (c) OMIT spectrum as a function of linearized coupling strength ω_{m2}. Other parameters are $\Delta = \omega_{m1}$, $\kappa/\omega_{m1} = 0.2$, $\gamma_1 = \gamma_2 = 10^{-5}\omega_{m1}$, $G_1/\omega_{m1} = 0.1$, $G_2/\omega_{m1} = 0.1$, $V/\omega_{m1} = 0.1$, and $\omega_{m1} = 10^8$ Hz.

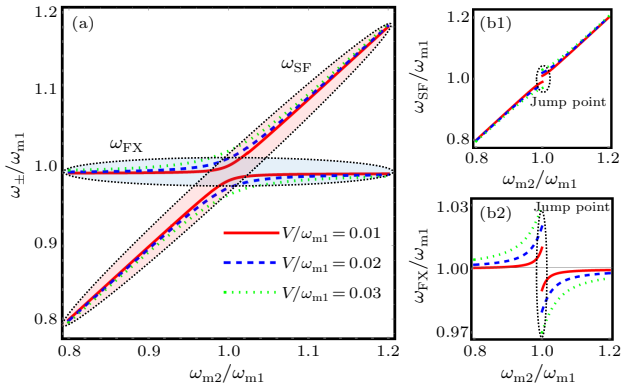


Fig. 3. The splitting fixed frequency ω_{FX} and shifted frequency ω_{SF} as a function of ω_{m2}. The jump point represents the change in sign of the frequency modification resulting from the frequency shift of ω_{m2}. Other parameters are the same as those in Fig. 2.

In Fig. 3, we investigate the relationship between the frequency of diagonalization and frequency change of the detection port. With the shift of ω_{m2}, the effective frequency ω_{FX} has small changes around ω_{m1}, but the effective frequency ω_{SF} has the significantly changes faraway from ω_{m1}. This is consistent with the analytical results in Ref. [10]. We plot the

changes of ω_{SF} and ω_{FX} with respect to ω_{m2} in Figs. 3(b1) and 3(b2), respectively. Under the given parameters, the difference between the two subgraphs is obvious, and ω_{SF} is more sensitive to ω_{m2}. This is also the difference between our model and the normal detection model.[47,48] We can incorporate the frequency change caused by the signal into one of the modes to simplify our detection process.

4. Mass sensor based on OMIT

In the process of mass detection, the mechanical oscillator is surround in a thermal environment, temperature increases the fluctuation of the detection port, and then reducing the detection accuracy of the system. OMIT is a frequency dependent coherent effect in optomechaincal systems. Compared with other effects in optomechanical systems, OMIT is more robust to the environment temperature. According to the analysis in the previous section, we can obtain that the mass of the adsorbed object will change the intrinsic frequency of the mechanical oscillator and then cause the frequency shift of the OMIT spectrum. The window or absorption peak of OMIT can be exhibited on the transmission spectrum. Thus, we can detect the mass by frequency shift of OMIT spectrum, which essentially avoids the problem that temperature affects the fluctuation of the signal strength. In this section, we show the protocol for detecting mass based on OMIT. According to the results in Fig. 3, ω_{SF} can directly reflect the mass of the probe port absorption (frequency change of ω_{m2}).

We show our detection protocol in Fig. 4, the mass of the adsorbed object is represented by the frequency shift of the OMIT spectrum at ω_{SF}. In the left subgraph of Fig. 4, we exhibit the change of OMIT spectrum with the mass of the adsorbed objects. It can be clearly seen that there are two distinct peak variation areas in the subgraph as the mass changes. One of the areas is not sensitive to changes in mass, which is around ω_{m1}. This corresponds exactly to the effect of ω_{FX} that we analyzed in Fig. 3. This area is not conducive to our detection scheme and needs to be avoided, so we mark it as a low-resolution region. The other area is more sensitive to changes in mass, and it corresponds to the effect of ω_{SF}. As discussed in Fig. 3, we note that this area is beneficial to detection. The frequency change caused by mass is linearly reflected in the change of the peak value in this area, so the mass can be deduced by analyzing the output spectrum. Similar conclusions were also given in Refs. [17,27,47,48]. In this area, OMIT induced output does not exhibit additional amplification (mass induced frequency shift is close to the frequency shift corresponding to OMIT output spectrum). The detection accuracy of this area strongly depends on the mass responsivity of the system, therefore, we mark it as a normal-resolution region. It should be noted that this area still belongs to the linear region of OMIT effect. However OMIT is typically a nonlinear effect, as shown in the subgraph at the lower right corner of Fig. 4, when $\delta \approx 0$, there is an obvious nonlinear effect between the peak value of the spectrum and the mass. The amplification effect of this region (see the slope of the red part) can reach infinity, so we mark it as a high-resolution region. In addition, although the abscissa marks the additional mass, it does not mean that we can only detect mass perturbations around 10 ag. We only need to set the mass of the second mechanical oscillator in advance to the value we need (such as the original mass plus 10 ag) to detect the attachment of a single small mass particle.

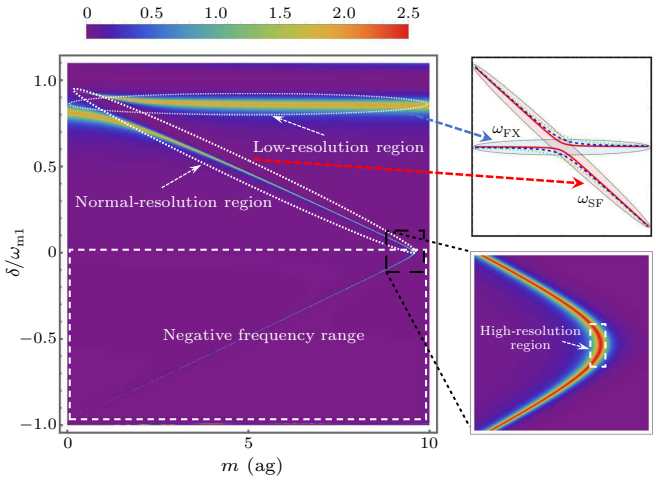


Fig. 4. The real part of χ as a function of δ and mass m (in units of ag $= 10^{-18}$ g). The negative frequency part of the figure is just to show our results better and will not be involved nor correspond to any physical meaning in our discussion. Other parameters are the same as those in Fig. 2.

Different from the traditional detection protocol, our protocol has no requirements for laser driving and optomechanical coupling strength in mass measurement, and our scheme can freely choose the detection accuracy according to the actual demand. If the requirements for precision are not high, select the normal-resolution region that is easier to achieve in terms of parameters. If the requirements for precision are high, select the high-resolution region that is sensitive to parameters. Our protocol does not rely on the presence of an OMIT window for detection; instead, it uses the real part of χ, specifically the absorption peak (highlighted in red in Fig. 4), to calibrate the mass to be measured. In the positive frequency region, the real part of χ remains below 2. However, in the negative frequency region, where the roles of the probe and driving fields are reversed, amplification occurs due to the driving, causing χ to exceed 2. In addition, compared to the OMIT detection protocol with a single resonator, our protocol is more robust to driving. Since we exploit the spectral properties of the double OMIT window induced by mode splitting due to coupling effects between the resonators. Although the spectrum is an output property of the probe field, the relative position of the OMIT spectra allows a perfect avoidance of

detection errors due to the frequency drift of the driving (the mechanical mode splitting is independent of the probe field frequency).

5. Discussion

In practical applications of our scheme, the system inevitably experiences the effects of environmental temperature and quantum fluctuations, which can diminish the detection accuracy. This noise may lead the detection system to misinterpret signals as mass, thereby limiting the lower bound of detectable mass accuracy in our scheme. When the mechanical quality factor $Q_{\rm m} \ll 1$, we can estimate the mass detection accuracy δm based on the equivalent mass of the noise action energy,[37,54]

$$\delta m \geq \frac{2m_2\gamma_2}{\omega_{\rm m2}}\sqrt{\frac{E_{\rm noise}}{E_{\rm c}}}, \tag{11}$$

where $E_{\rm c} \approx m_2\omega_{\rm m2}^2\langle q_2\rangle_0^2$ represents the maximum driving energy and $E_{\rm noise} = k_{\rm B}T + \hbar g_2(\langle a_{\rm in}^{\dagger}a_{\rm in}\rangle + \langle a_{\rm in}a_{\rm in}^{\dagger}\rangle)$ accounts for the sum of thermal energy from the probe port mode and fluctuation energy of the optical mode. Here, $k_{\rm B}$ is the Boltzmann constant, T is the environmental temperature, and m_2 denotes the mass of the mechanical oscillator 2. We utilize a membrane optomechanical system capable of constructing two-oscillator couplings to demonstrate the detection capabilities of our protocol with a characteristic mass $m \approx 10^{-6}$ g.[49] The minimum detection mass is plotted as a function of temperature and dissipation in Fig. 5. It is observed that as temperature and dissipation increase, the minimum detection mass also rises, indicating reduced precision in our detection protocol. Under the current experimental conditions, it is feasible to achieve a resonator temperature below 1 K and dissipation $\kappa/\omega_{\rm m2} = 0.1$, resulting in a detection precision of $\delta m \approx 204.8$ zg (204.8×10^{-21} g). This precision is significantly lower than the mass discussed in Fig. 5, i.e., ag (10^{-18} g). At room temperature (300 K), the detection accuracy is $\delta m \approx 3547.7$ zg, which can also achieve a level of ag.

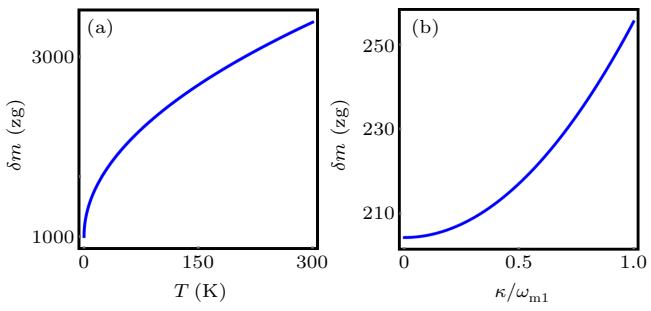


Fig. 5. (a) Minimum detection mass as a function of temperature with $\kappa/\omega_{\rm m1} = 0.2$. (b) Minimum detection mass as a function of optical dissipation with $T = 1$ K. Other parameters are $V/\omega_{\rm m} = 0.1$, $\gamma_1 = \gamma_2 = 10^{-5}\omega_{\rm m1}$, $g_1 = g_2 = 10^{-3}\omega_{\rm m}$, $\varepsilon_{\rm c}/\omega_{\rm m1} = 20$, $m = 10^{-6}$ g.

6. Conclusion

In conclusion, we propose a tiny mass detection scheme based on OMIT effect. The detection accuracy of this detection scheme can be adjusted by changing the mass of the second oscillator. We can achieve normal-resolution detection with the same accuracy as reported in recent works,[17,27,47,48] and high-resolution detection with much higher accuracy. All the parameters we selected are within the range that can be reached in the present experiment.[55] In Fig. 4, for the sake of demonstration, the detection quantity we choose is the absorption peak value. From the analysis in Fig. 2, we can see that if OMIT window is used as a probe, similar conclusion still holds. Since we are detecting frequency shifts, the protocol is valid only if the signal is distinguishable from the thermal noise, and such schemes for detecting frequency shifts are robust to temperature.[37] In addition, in our analysis in Fig. 2, we can also see that if the OMIT window is used as a probe, the disturbance of the system to the driving laser is also robust. Our scheme provides a new way to detect small masses with high precision, and is robust to temperature as well as driving laser disturbance. It provides a potentially valuable platform for quality detection and its application.

Acknowledgments

We thank Cheng Jiong for instructive discussions. Project supported by the Science Foundation of Zhejiang Sci-Tech University (Grant No. 18062145-Y), the National Natural Science Foundation of China (Grant Nos. 12075209 and 12074206), the Natural Science Foundation of Zhejiang Province (Grant No. LY22A040005), and the Innovation Program for Quantum Science and Technology (Grant No. 2023ZD0300904).

References

[1] Parikh M, Wilczek F and Zahariade G 2021 *Phys. Rev. Lett.* **127** 081602
[2] Marletto C and Vedral V 2017 *Phys. Rev. Lett.* **119** 240402
[3] Ma Y, Danilishin S L, Zhao C, Miao H, Korth W Z, Chen Y, Ward R L and Blair D G 2014 *Phys. Rev. Lett.* **113** 151102
[4] Crescini N, Alesini D, Braggio C, Carugno G, D'Agostino D, Di Gioacchino D, Falferi P, Gambardella U, Gatti C, Iannone G, Ligi C, Lombardi A, Ortolan A, Pengo R, Ruoso G and Taffarello L QUAX Collaboration 2020 *Phys. Rev. Lett.* **124** 171801
[5] Ye J and Zoller P 2024 *Phys. Rev. Lett.* **132** 190001
[6] Estrada J, Harnik R, Rodrigues D and Senger M 2021 *PRX Quantum* **2** 030340
[7] Lopaeva E D, Ruo Berchera I, Degiovanni I P, Olivares S, Brida G and Genovese M 2013 *Phys. Rev. Lett.* **110** 153603
[8] Lloyd S 2013 *Science* **321** 1463
[9] Barzanjeh S, Guha S, Weedbrook C, Vitali D, Shapiro J H and Pirandola S 2015 *Phys. Rev. Lett.* **114** 080503
[10] Xu X and Taylor J M 2014 *Phys. Rev. A* **90** 043848
[11] Zhang W Z, Chen L B, Cheng J and Jiang Y F 2019 *Phys. Rev. A* **99** 063811
[12] Liu Z, Liu Y Q, Mai Z Y, Yang Y J, Zhou N n and Yu C S 2024 *Phys. Rev. A* **109** 023709
[13] Zhang K, Bariani F, Dong Y, Zhang W and Meystre P 2015 *Phys. Rev. Lett.* **114** 113601

[14] Rong X, Jiao M, Geng J, Zhang B, Xie T, Shi F, Duan C K, Cai Y F and Du J 2018 *Phys. Rev. Lett.* **121** 080402
[15] Rugar D, Budakian R, Mamin H J and Chui B W 2004 *Nature* **430** 329
[16] Lecocq F, Teufel J D, Aumentado J and Simmonds R W 2015 *Nat. Phys.* **11** 635
[17] Li J J and Zhu K D 2012 *Appl. Phys. Lett.* **101** 141905
[18] Lecocq F, Clark J B, Simmonds R W, Aumentado J and Teufel J D 2015 *Phys. Rev. X* **5** 041037
[19] Aspelmeyer M, Kippenberg T J and Marquardt F 2014 *Rev. Mod. Phys.* **86** 1391
[20] Peano V, Schwefel H G L, Marquardt C and Marquardt F 2015 *Phys. Rev. Lett.* **115** 243603
[21] Xia Y, Agrawal A R, Pluchar C M, Brady A J, Liu Z, Zhuang Q, Wilson D J and Zhang Z 2023 *Nat. Photon.* **17** 470
[22] Wang C W, Niu W, Zhang Y, Cheng J and Zhang W Z 2023 *Opt. Express* **31** 11561
[23] Li K, Davuluri S and Li Y 2018 *Chin. Phys. B* **27** 084203
[24] Wu M, Hryciw A C, Healey C, Lake D P, Jayakumar H, Freeman M R, Davis J P and Barclay P E 2014 *Phys. Rev. X* **4** 021052
[25] Shapiro J H 2020 *IEEE Aerospace and Electronic Systems Magazine* **35** 8
[26] Regal C A, Teufel J D and Lehnert K W 2008 *Nat. Phys.* **4** 555
[27] He Y 2015 *Appl. Phys. Lett.* **106** 121905
[28] Liu F, Alaie S, Leseman Z C and Hossein-Zadeh M 2013 *Opt. Express* **21** 19555
[29] Yang Y T, Callegari C, Feng X L, Ekinci K L and Roukes M L 2006 *Nano Lett.* **6** 583
[30] Motazedifard A, Bemani F, Naderi M H, Roknizadeh R and Vitali D 2016 *New J. Phys.* **18** 073040
[31] Allahverdi H, Motazedifard A, Dalafi A, Vitali D and Naderi M H 2022 *Phys. Rev. A* **106** 023107
[32] Singh V, Bosman S J, Schneider B H, Blanter Y M, Castellanos-Gomez A and Steele G A 2014 *Nat. Nanotechnol.* **9** 820
[33] Cole G D, Wilson-Rae I, Werbach K, Vanner M R and Aspelmeyer M 2011 *Nat. Commun.* **2** 231
[34] Imamoglu A and Whaley K B 2015 *Phys. Rev. E* **91** 022714
[35] Baake E, Baake M and Wagner H 1998 *Phys. Rev. E* **57** 1191
[36] York D M, Lee T S and Yang W 1998 *Phys. Rev. Lett.* **80** 5011
[37] Liu J and Zhu K D 2018 *Photonics Research* **6** 867
[38] Agarwal G S and Huang S 2010 *Phys. Rev. A* **81** 041803
[39] Shen Z, Zhang Y L, Chen Y, Zou C L, Xiao Y F, Zou X B, Sun F W, Guo G C and Dong C H 2016 *Nat. Photon.* **10** 657
[40] Jing H, Özdemir c K, Geng Z, Zhang J, Lü X Y, Peng B, Yang L and Nori F 2015 *Scientific Reports* **5** 9663
[41] Agarwal G S and Jha S S 2013 *Phys. Rev. A* **88** 013815
[42] Massel F, Cho S U, Pirkkalainen J M, Hakonen P J, Heikkilä T T and Sillanpää M A 2012 *Nat. Commun.* **3** 987
[43] Weis S, Rivière R, Deléglise S, Gavartin E, Arcizet O, Schliesser A and Kippenberg T J 2010 *Science* **330** 1520
[44] Karuza M, Biancofiore C, Bawaj M, Molinelli C, Galassi M, Natali R, Tombesi P, Di Giuseppe G and Vitali D 2013 *Phys. Rev. A* **88** 013804
[45] Zhou X, Hocke F, Schliesser A, Marx A, Huebl H, Gross R and Kippenberg T J 2013 *Nat. Phys.* **9** 179
[46] Peng J X, Chen Z, Yuan Q Z and Feng X L 2019 *Phys. Rev. A* **99** 043817
[47] Wang Q, Li W J, Ma P C and He Z 2017 *International Journal of Theoretical Physics* **56** 2212
[48] Wang Q and Li W J 2017 *International Journal of Theoretical Physics* **56** 1346
[49] Patil Y S, Chakram S, Chang L and Vengalattore M 2015 *Phys. Rev. Lett.* **115** 017202
[50] Lassagne B, Garcia-Sanchez D, Aguasca A and Bachtold A 2008 *Nano Lett.* **8** 3735
[51] Li W, Li C and Song H 2017 *Phys. Rev. A* **95** 023827
[52] Scully M O and Zubairy M S 1997 *Quantum Optics* (Cambridge: Cambridge University Press)
[53] Mu Q X, Lang C and Zhang W Z 2019 *Chin. Phys. B* **28** 114206
[54] Ekinci K L, Yang Y T and Roukes M L 2004 *J. Appl. Phys.* **95** 2682
[55] Chen Y, Zhang Y L, Shen Z, Zou C L, Guo G C and Dong C H 2021 *Phys. Rev. Lett.* **126** 123603